Doping fluctuation-driven magneto-electronic phase separation in $La_{1-x}Sr_xCoO_3$ single crystals

2009 EPL 87 27006

(http://iopscience.iop.org/0295-5075/87/2/27006)

A Letters Journal Exploring the Frontiers of Physics

July 2009

EPL, **87** (2009) 27006 www.epljournal.org
doi: 10.1209/0295-5075/87/27006

Doping fluctuation-driven magneto-electronic phase separation in $La_{1-x}Sr_xCoO_3$ single crystals

C. He[1], S. El-Khatib[1,2], J. Wu[1], J. W. Lynn[2], H. Zheng[3], J. F. Mitchell[3] and C. Leighton[1(a)]

[1] *Department of Chemical Engineering and Materials Science, University of Minnesota Minneapolis, MN 55455, USA*
[2] *NIST Center for Neutron Research, National Institute for Standards and Technology Gaithersburg, MD 20899, USA*
[3] *Materials Science Division, Argonne National Laboratory - Argonne, IL 60439, USA*

received 5 June 2009; accepted in final form 9 July 2009
published online 5 August 2009

PACS 75.30.Kz – Magnetic phase boundaries (including magnetic transitions, metamagnetism, etc.)
PACS 71.30.+h – Metal-insulator transitions and other electronic transitions
PACS 72.15.Gd – Galvanomagnetic and other magnetotransport effects

Abstract – In recent years it has become clear that complex oxides provide an exceptional platform for the discovery of new physics as well as a considerable challenge to our understanding of correlated electrons. The tendency of these materials to display nanoscale electronic and magnetic inhomogeneity is a good example. Here, we have applied a variety of experimental techniques to investigate this magneto-electronic phase separation in a model system —the doped cobaltite $La_{1-x}Sr_xCoO_3$. Comparing experimental data over a wide range of doping with statistical simulations, we conclude that the magneto-electronic inhomogeneity is driven solely by inevitable local compositional fluctuations at nanoscopic length scales. The phase separation is thus doping fluctuation-driven rather than electronically driven, meaning that more complex electronic phase separation models are not required to understand the observed phenomena in this material.

Magneto-electronic phase separation (MEPS), the spatial coexistence of multiple electronic and magnetic phases even in the absence of chemical segregation, is ubiquitous in complex oxides such as cuprates and manganites, and is considered key to understanding some of their most important properties [1,2]. The effect is an excellent example of the phenomena that emerge from the interplay between the active degrees of freedom in such oxides [1–4], which result in a delicate energy balance between phases. In magnetic oxides intrinsic inhomogeneities have been observed by neutron scattering [5–8], nuclear magnetic resonance (NMR) [9,10], scanning tunneling spectroscopy [11–13], magnetic microscopy [14,15], and many other probes, and are the subject of intense theoretical work. It is now understood that nanoscopic electronic phase separation occurs in many models of relevance to the manganites (*e.g.* one- and two-orbital double-exchange models) [1,2,16,17], while mesoscopic MEPS is found when quenched disorder is included near a 1st-order phase boundary [1,2,18]. Strain-based models have also been advanced [19], and can explain multiple length scales in a single framework.

Experimentally, the perovskite cobaltites have proven useful in the study of MEPS. The $La_{1-x}Sr_xCoO_3$ (LSCO) system has been intensively studied and is well established (from neutron diffraction [20], NMR [21], Small-Angle Neutron Scattering (SANS) [22], and inelastic neutron spectroscopy [23,24]) to phase-separate into nanoscopic ferromagnetic (FM) clusters in a non-FM matrix at low x. As x increases the clusters percolate, leading to a crossover from short- to long-range FM at $x_C \approx 0.18$ [22]. LSCO offers several attractive features for fundamental studies including nanoscopic length scales [22–24] (as in electronic phase separation, where length scales are limited by Coulomb interactions), isotropic clusters [23], doping-tunable cluster density, similar crystal structures for clusters and matrix, and the absence of long-range antiferromagnetic (AF) order at low doping, which simplifies detection of FM clusters. We show here that a detailed study of magnetic cluster sizes and phase

(a) E-mail: leighton@umn.edu

fractions in LSCO single crystals yields the unanticipated result that the MEPS is confined to a well-defined doping range, $0.04 < x < 0.22$. This exact range, as well as the x-dependence of the phase fractions, can be perfectly reproduced by simple statistical simulations based on the local doping fluctuations that must occur in any randomly doped solid on these nanoscopic length scales. MEPS in LSCO is therefore doping fluctuation-driven as opposed to electronically driven. We conclude that in this system, and perhaps others exhibiting *nanoscopic* phase separation in parts of their phase diagrams, more complex electronic phase separation models may not be required.

LSCO crystals [22–26] of 12 compositions ($0.00 \leqslant x \leqslant 0.30$), were grown by floating zone methods and proven single crystal/single phase by X-ray and neutron diffraction. SANS was performed at the NIST Center for Neutron Research at a wavelength of 6–8 Å, in the wave vector range $0.003\,\text{Å}^{-1} < q < 0.2\,\text{Å}^{-1}$. Absolute cross-sections were determined, and the magnetic contribution was isolated by subtracting the scattering at high temperatures (>300 K). Heat capacity was measured via the relaxation method in a commercial system (Quantum Design) from 0.35 K to 270 K in fields to 9 T.

We first discuss the basic features of the SANS data in order to introduce the most important aspects of the phenomenology. Figures 1(a)–(c), plot the T-dependence of the low scattering wave vector ($q = 0.007\,\text{Å}^{-1}$) intensity ($[\mathrm{d}\Sigma/\mathrm{d}\Omega]_{low\,q}$), high-$q$ ($0.049\,\text{Å}^{-1}$) scattering intensity ($[\mathrm{d}\Sigma/\mathrm{d}\Omega]_{high\,q}$), and magnetic correlation length, ξ, for 4 representative single-crystal samples. $x = 0.30$ and 0.22 crystals show the onset of low-q scattering and a peak in $[\mathrm{d}\Sigma/\mathrm{d}\Omega]_{high\,q}$ at the Curie temperature, T_C. $[\mathrm{d}\Sigma/\mathrm{d}\Omega]_{low\,q}$ follows the Porod form ($\mathrm{d}\Sigma/\mathrm{d}\Omega \propto q^{-4}$) due to scattering from domains of size D, in the limit $q \gg 2\pi/D$ [22]. Adherence to this form down to $q = 0.003\,\text{Å}^{-1}$ immediately implies that the domains exceed 2000 Å, *i.e.* truly long-range FM order [22–24]. $[\mathrm{d}\Sigma/\mathrm{d}\Omega]_{high\,q}$, on the other hand, is Lorentzian ($\mathrm{d}\Sigma/\mathrm{d}\Omega \propto 1/(q^2 + (1/\xi)^2)$), enabling extraction of the magnetic correlation length [22]. As shown in fig. 1(c), for $x = 0.30$ and $0.22\,\xi$ diverges as $T \to T_C^+$, as expected in a long-range-ordered FM. At $x = 0.17$, which is very close to the percolation threshold, x_C, ξ diverges as $T \to T_C^+$ and the low-q scatter shows a clear onset, but $[\mathrm{d}\Sigma/\mathrm{d}\Omega]_{high\,q}$ has only a bump at T_C with significant intensity at low T. The $x = 0.15$ crystal ($x < x_C$) is radically different. $[\mathrm{d}\Sigma/\mathrm{d}\Omega]_{low\,q}$ is negligible, while $[\mathrm{d}\Sigma/\mathrm{d}\Omega]_{high\,q}$ shows an onset around 150 K, becoming intense at low T. Consistent with the negligible low-q scattering, ξ does not diverge. Apparently spin correlations emerge at ∼150 K, grow in range with decreasing T, but are limited to ∼ 2.5 nm by the physical size of the magnetic clusters. We thus use ξ, which strictly provides a measure of the characteristic spatial extent of the spin correlation function, as an approximate measure of the FM droplet size. The validity of this procedure is borne out by the reasonable agreement with the ξ values derived from elastic neutron scattering peak widths [23]. For $x \leqslant 0.15$,

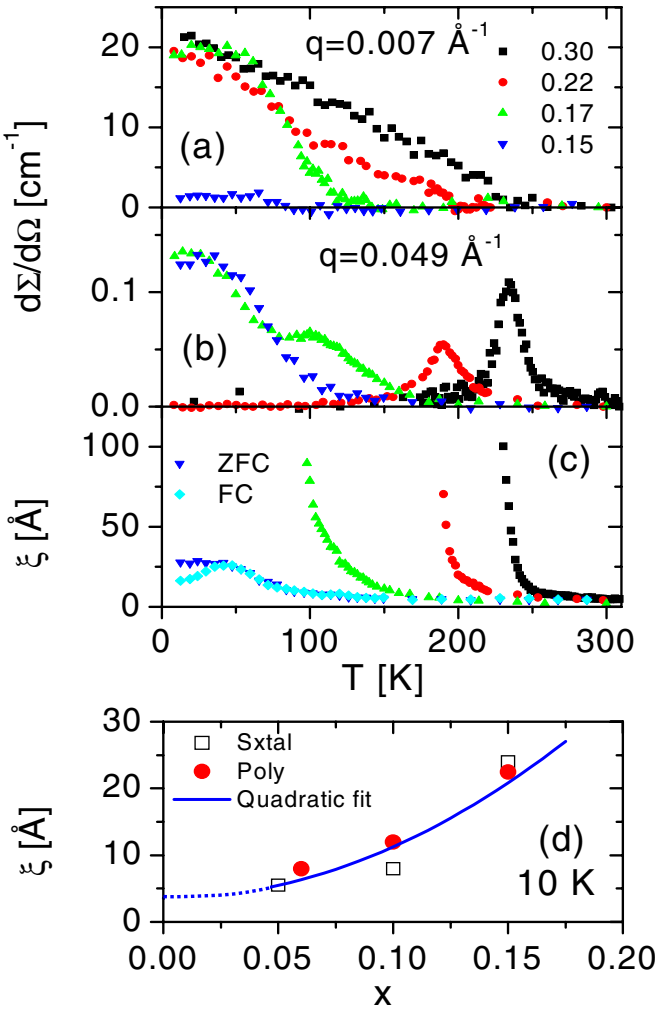

Fig. 1: (Color online) T dependence of the magnetic SANS intensity (absolute cross-section) at $q = 0.007\,\text{Å}^{-1}$ (a) and $q = 0.049\,\text{Å}^{-1}$ (b) and the extracted magnetic correlation length (c) for $x = 0.15$, 0.17, 0.22 and 0.30 single crystals. The bottom panel (d) shows the x-dependence of the magnetic correlation length for both single- and poly-crystals at 10 K.

$\xi(T)$ shows a splitting between field-cooled (FC) and zero-field-cooled (ZFC) curves close to the "spin-glass" freezing temperature [26]. The doping dependence of ξ for both single- and poly-crystals (fig. 1(d)) shows a weak increase with increasing x, from ∼ 2 unit cells (6–8 Å) at $x = 0.05$ up to ∼ 6 unit cells (20–25 Å) at $x = 0.15$, an important point for the analysis presented below.

Figures 2(a,b) show the low-T (10 K) SANS intensities *vs.* x. $[\mathrm{d}\Sigma/\mathrm{d}\Omega]_{low\,q}$ is negligible at low x due to the absence of long-range FM, but turns on at $x = 0.17$, *i.e.* at percolation. A maximum occurs at $x = 0.20$ due to formation of a percolated network with maximum contrast between FM and non-FM phases. Significantly, $[\mathrm{d}\Sigma/\mathrm{d}\Omega]_{low\,q}$ becomes roughly constant above $x = 0.22$, at a lower value than at $x = 0.20$. The surprising implication is that a uniform single-phase FM state is entered at $x \geqslant 0.22$, at which point $[\mathrm{d}\Sigma/\mathrm{d}\Omega]_{low\,q}$ comes only from

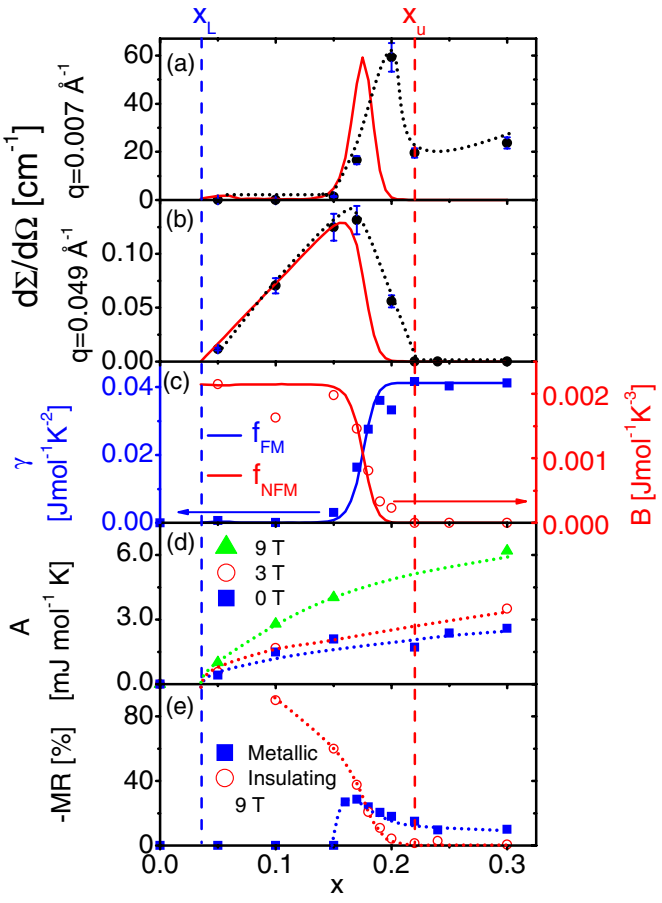

Fig. 2: (Color online) Doping dependence of the 10 K magnetic SANS intensity (absolute cross-section) at (a) $q = 0.007$ Å^{-1} and (b) $q = 0.049$ Å^{-1}. Doping dependence of the electronic and T^2 contributions to the specific heat (c), the nuclear hyperfine contribution to the specific heat (d), and the 9 T magnetoresistance (e). The dotted lines are guides to the eye while the solid lines are fits to the models described in the text. The vertical dashed lines indicate the upper and lower limits for the phase separation, x_U and x_L.

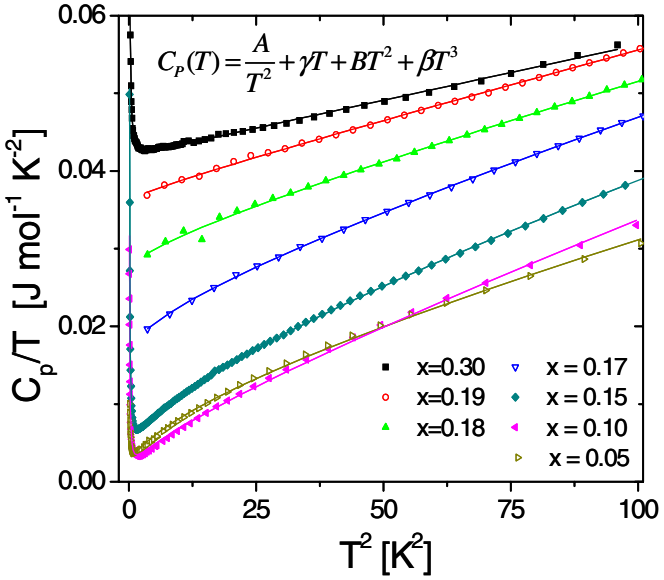

Fig. 3: (Color online) T-dependence of the specific heat plotted as C_P/T *vs.* T^2 for single crystals with $x = 0.05$, 0.10, 0.15, 0.17, 0.18, 0.19, and 0.30. The solid lines are fits to the equation shown in the figure and described in the text.

domains. The x-dependence of $[d\Sigma/d\Omega]_{high\,q}$ (fig. 2(b)) strengthens this argument. Not only does $[d\Sigma/d\Omega]_{high\,q}$ vanish at $x = 0.22$ (the point at which $[d\Sigma/d\Omega]_{low\,q}$ flattens), but also as $x \to 0.04$, the first strong evidence that the MEPS in LSCO is confined to a specific doping range. FM-correlated nanoscopic clusters apparently first form at statistically significant density at $x = 0.04$, increase in scattering intensity up to $x = 0.15$, decrease beyond $x = 0.17$ due to coalescence, then become negligible at $x = 0.22$ when uniform FM is established.

Further evidence for a finite range over which MEPS occurs is provided by the specific heat, C_P. Figure 3 shows $C_P(T)$ ($0.35\,\mathrm{K} < T < 10\,\mathrm{K}$) plotted as C_P/T *vs.* T^2 (for 7 representative samples) to test the relation $C_P(T) = \gamma T + \beta T^3$. The electronic contribution, γ, is given in a free electron model by $\gamma = \pi^2 k_B^2 N(E_F)/3$, where $N(E_F)$ is the density of states at the Fermi level. The lattice contribution, β, is given in the Debye model by $\beta = 234 N k_B/\Theta_D^3$, where N is the number of ions/mole and Θ_D is the Debye temperature. Considering first the data at $T > 2\,\mathrm{K}$ and $x = 0.30$ (*i.e.* deep in the FM metallic phase), we see that this form is indeed valid[1], although with a large γ which we will discuss elsewhere. As x is decreased the intercept in fig. 3 (*i.e.* γ) decreases (due to the approach to the metal-insulator transition), but is accompanied by significant downward curvature at low T. To quantify this additional contribution to $C_P(T)$, a term of the form BT^α was included, with α allowed to vary with x. Such fits produced $\alpha = 2.10 \pm 0.16$, strong evidence for a BT^2 contribution. $C_P(T) = \gamma T + \beta T^3 + BT^2$ provides a good fit to the data (solid lines). The extracted $\gamma(x)$ and $B(x)$ are shown in fig. 2(c). $\gamma = 0$ at low x, increases rapidly at x_C then saturates at $x = 0.22$, further evidence for the existence of a homogeneous FM metallic state above $x = 0.22$. The second remarkable feature is the form of $B(x)$, which is essentially reciprocal to $\gamma(x)$; B is constant below $x = 0.15$, then falls smoothly to zero at $x = 0.22$. It is thus clear that the BT^2 term must originate in the non-FM phase, *i.e.* what we observe in $\gamma(x)$ and $B(x)$ is essentially phase conversion from non-FM to FM with increasing x. Note that a T^2 term in C_P has been identified in $LaMnO_3$ [27], and ascribed to A-type AF order. Although LSCO is not AF at low x, simultaneous F and AF spin correlations have been found, consistent with A-type AF fluctuations [23]. Moreover, it has been generally argued [28] that phase-separated systems with

[1] Absence of an FM spin-wave contribution is understood in terms of the magnetocrystalline anisotropy which results in a gapped spin wave excitation spectrum.

both F and AF interactions have long-wavelength spin excitations producing a T^2 term in heat capacity, an argument that could be applicable here also. In any case, and regardless of the exact mechanism, the spatial origin of the BT^2 term is clear; it arises in the non-FM phase.

Consider now the low-T data (*i.e.* below 2 K). The upturn in C_P/T at low T (only 4 curves are shown for clarity) is common in magnetic materials and is due to a nuclear hyperfine contribution [1,27,28]. Internal magnetic fields Zeeman split the nuclear energy levels ($\Delta E = 2\mu_{nuc}H_{hf}$, where μ_{nuc} is the nuclear moment, H_{hf} is the hyperfine field, and we have used nuclear spin, $I = 1/2$ for illustration), leading to a Schottky anomaly which, in the limit $T \gg \Delta E$, is approximated by $C_P(T) = A/T^2$, where $A \propto H_{hf}^2$ [1,27,28]. The solid lines in fig. 3 include this contribution, confirming that it is a good description of the data. The doping dependence of A (fig. 2(d)) reveals large values at high x (equivalent to $H_{hf} \approx 16$ T, consistent with zero field Co NMR [21]), which persist to $x < 0.18$ (due to the local internal field in the clusters), eventually vanishing as $x \to 0.04$. This is in remarkable agreement with the SANS data of fig. 2(b), further evidence for the appearance of FM clusters in significant density at $x \approx 0.04$. Note that the applied field dependence of $A(x)$ (fig. 2(d)), is consistent with an FM internal field, and rules out the possibility of paramagnetic defects as the origin of the Schottky anomaly. Magnetotransport (fig. 2(e)) provides further confirmation. As described previously [25], the magnetoresistance can be simply decomposed into "metallic" and "insulating" contributions. The insulating contribution disappears at $x = 0.22$, at which point the metallic contribution becomes constant, confirming once more the onset of uniform FM beyond $x = 0.22$. This conclusion is also consistent with La NMR showing a saturation of the center field of the resonance near $x = 0.22$ [29].

Given such clear evidence of localization of the phase-separated region to a specific range of doping either side of the percolation transition, simulations were performed to determine if this finite range could possibly be accounted for by local doping fluctuations. A $240 \times 240 \times 240$ array of La ions was considered. Doping was achieved by assigning a probability x of occupation of a given site with Sr and the lattice was broken up into sampling volumes ξ^3, playing the role of the nanoscopic clusters. The distribution in local dopings on the sampling length scale ξ, $P(x_{local})$, was then collected at multiple global doping values, x. As an illustration, the distributions arising for sampling volumes of 3 unit cells cubed and 11 unit cells cubed are shown as color plots in figs. 4(a) and (b). Vertical cuts through these figures are the $P(x_{local})$ distributions at that particular global x value. The width of these distributions is obviously dependent on the sampling volume, decreasing dramatically from fig. 4(a) to fig. 4(b). Consider the intersection of these distributions with the horizontal line $x_{local} = 0.18$, *i.e.* x_C from the *bulk* phase diagram. Assuming that in any region with $x_{local} > 0.18$ FM order is stable (leading to nucleation of a short-range FM cluster), and in any region with $x_{local} < 0.18$ FM order is unstable, leads to prediction of a finite range for MEPS. The lower intersection point, x_L, is the point at which the entire distribution is below $x_{local} = 0.18$ (a uniform non-FM state), and the upper intersection point, x_U, is the point at which the entire distribution lies above $x_{local} = 0.18$ (a uniform FM state). Figures 4(a) and (b) thus predict $x_L = 0.06$, $x_U = 0.36$, and $x_L = 0.14$, $x_U = 0.21$, respectively, neither of which agree with experiment. This is because, as shown in fig. 1(d), the actual experimentally determined sampling length scale (*i.e.* the magnetic correlation length) is itself dependent on global doping. $\xi(x)$ was therefore fitted to a simple function (a quadratic, fig. 1(d)) in order to compute the relevant sampling length at any x as an input for the simulations. As an aside, note that i) a quadratic describes $\xi(x)$ better than a linear function, and ii) finite $\xi(x \to 0)$ can be rationalized in terms of non-zero spin states in magnetic excitons [30,31] or spin-state polarons [32], which could be the precursors to the FM correlated clusters we observe at $x \geqslant 0.04$. Local magnetic entities such as polarons [24,32] or magnetic excitons [30,31] likely exist at very low (even zero) x, but strongly FM-correlated spin clusters apparently first form at $x \approx 0.04$. The results from these final simulations are shown in fig. 4 (c). The unusual shape of the distribution is due to the form of $\xi(x)$. At low x the distribution is wide due to the small sampling volume (~ 2 unit cells cubed), while at high x it is narrow due to the larger sampling volume. From fig. 4(c) we predict $x_L = 0.03$, $x_U = 0.21$, remarkably close to the experimental values (0.04 and 0.22). *Note that this agreement is achieved with no adjustable parameters, using the experimentally determined* $\xi(x)$.

The validity of the model can be further verified by extracting the phase fractions, f_{FM} (of the long-range-ordered FM phase) and f_{NFM}. These are shown in fig. 2(c), normalized to, and overlaid on, $\gamma(x)$ and $B(x)$, which we have argued must scale with f_{FM} and f_{NFM}. The agreement is satisfactory. The x-dependence of $[\mathrm{d}\Sigma/\mathrm{d}\Omega]_{high\,q}$ (fig. 2(b)) can also be modeled. $[\mathrm{d}\Sigma/\mathrm{d}\Omega]_{high\,q}$ must be proportional to the phase fraction of the non-long-range-ordered regions (f_{NFM}) and the density of clusters within these regions, which we observed to increase linearly with x beyond $x = 0.04$, *i.e.* $[\mathrm{d}\Sigma/\mathrm{d}\Omega]_{high\,q} = C(x - 0.04)f_{NFM}(x)$, where C is a constant. As shown in fig. 2(b) the agreement with experiment is reasonable. $[\mathrm{d}\Sigma/\mathrm{d}\Omega]_{low\,q}$ is of the Porod type and is thus proportional to the specific area of contact between FM and non-FM phases. This can be crudely approximated as $[\mathrm{d}\Sigma/\mathrm{d}\Omega]_{low\,q} \approx C' f_{FM}(x) f_{NFM}(x)$ (C' is a constant) [33], which is exact as $f_{FM} \to 0$, 1. As shown in fig. 2(a) the simulation (solid line) faithfully reproduces the onset at $x = 0.15$, and the peak near percolation, but is incapable of modeling the constant intensity at $x \geqslant 0.22$, which arises from domains.

The striking agreement between experiment and these simple statistical simulations directly implies that the phase-separated state in LSCO can be explained solely on the basis of unavoidable local doping fluctuations

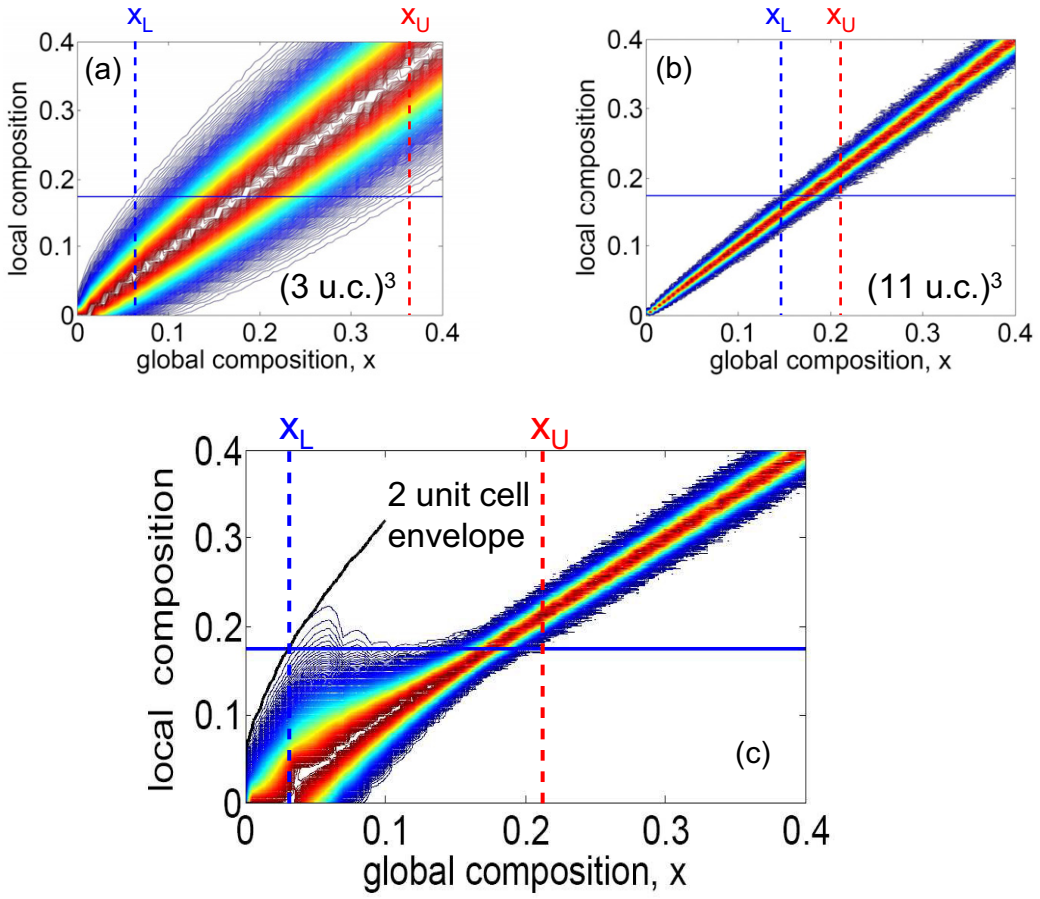

Fig. 4: (Color online) Calculated distribution of local doping as a function of the global doping, x, for sampling volumes of (a) 3 unit cells cubed, (b) 11 unit cells cubed, and (c) the experimentally determined (x-dependent) magnetic correlation volume. The vertical lines indicate the upper and lower limits for the phase separation, *i.e.* the points where the distributions intersect the horizontal line at $x = 0.18$.

in a randomly doped crystal, with no need to invoke electronic phase separation. It is important to stress that electronic inhomogeneity is of course still present. It is simply driven by doping fluctuations as opposed to an electronically driven phase separation mechanism. The long-range Coulomb interaction likely plays a key role in limiting the phase separation length scale (see ref. [17] for example), making these local compositional fluctuations extremely important. It is clear that longer length scale inhomogeneities, (which seem to occur in some manganites for example) cannot be described by this model, as can be seen from the rapid decrease in distribution width with sampling volume. As a final comment note that a key feature of this analysis is that the critical doping level for the onset of FM order in the *bulk* phase diagram ($x = 0.18$) apparently applies at surprisingly short length scales, of the order of only 2 unit cells.

In summary, we made a detailed study of the nanoscale magneto-electronic phase separation in single crystal $La_{1-x}Sr_xCoO_3$, revealing the existence of a specific range over which it occurs. This exact doping range, the doping dependence of the phase fractions, and the doping dependence of the small-angle neutron scattering, can all be reproduced by simple statistical simulations incorporating the local compositional fluctuations that must occur on nanoscopic length scales. The magneto-electronic phase separation is therefore driven by spatial fluctuations in doping rather than true electronic phase separation. Similar mechanisms could be at work in other randomly doped oxides exhibiting magneto-electronic inhomogeneity (*e.g.* cuprates and manganites), provided that the coexisting phases have sufficiently small free energy differences, and, crucially, that the inhomogeneities occur on truly nanoscopic length scales.

* * *

Neutron scattering supported by DoE (DE-FG02-06ER46275). Additional UMN funding from NSF (DMR-0804432) and the Dept. of Commerce (6D6146). Neutron experiments utilized facilities supported in part by NSF (DMR-0454672). CL thanks M. Hoch, W. Moulton, and I. Terry for useful discussions.

REFERENCES

[1] Dagotto E., *Nanoscale Phase Separation and Colossal Magnetoresistance* (Springer, New York) 2002.

[2] Dagotto E., Hotta T. and Moreo A., *Phys. Rep.*, **344** (2001) 1.

[3] Tokura Y. and Tomioka Y., *J. Magn. & Magn. Mater.*, **200** (1999) 1.

[4] Coey J. M. D., Viret M. and von Molnár S., *Adv. Phys.*, **48** (1999) 167.

[5] Lynn J. W., Erwin R. W., Borchers J. A., Huang Q., Santoro A., Peng J.-L. and Li Z. Y., *Phys. Rev. Lett.*, **76** (1996) 4046.

[6] Hennion M., Moussa F., Biotteau G., Rodriguez-Carvajal J., Pinsard L. and Revcolevschi A., *Phys. Rev. Lett.*, **81** (1998) 1957.

[7] Granado E., Ling C. D., Neumeier J. J., Lynn J. W. and Argyriou D. N., *Phys. Rev. B*, **68** (2003) 134440.

[8] Simon Ch., Mercone S., Guiblin N., Martin C., Brulet A. and Andre G., *Phys. Rev. Lett.*, **89** (2002) 207202.

[9] Papavassiliou G., Fardis M., Belesi M., Maris T. G., Kallias G., Pissas M., Niarchos D., Dimitropoulos C. and Dolinsek J., *Phys. Rev. Lett.*, **84** (2000) 761.

[10] Savosta M. M. and Novak P., *Phys. Rev. Lett.*, **87** (2001) 137204.

[11] Fath M., Freisem S., Menovsky A. A., Tomioka Y., Aarts J. and Mydosh J. A., *Science*, **285** (1999) 1540.

[12] Renner Ch., Aeppli G., Kim B.-G., Soh Y. and Cheong S. W., *Nature*, **416** (2002) 518.

[13] Ma J. X., Gillaspie D. T., Plummer E. W. and Shen J., *Phys. Rev. Lett.*, **95** (2005) 237210.

[14] Asaka T., Anan Y., Nagai T., Tsutsumi S., Kuwahara H., Kimoto K., Tokura Y. and Matsui Y., *Phys. Rev. Lett.*, **89** (2002) 207203.

[15] Tokunaga M., Tokunaga Y. and Tamegai T., *Phys. Rev. Lett.*, **93** (2004) 037203.

[16] Kumar S. and Majumdar P., *Phys. Rev. Lett.*, **92** (2004) 126602.

[17] Kugel K. I., Rakhmanov A. L. and Sboychakov A. O., *Phys. Rev. Lett.*, **95** (2005) 267210.

[18] Burgy J., Mayr M., Martin-Mayor V., Moreo A. and Dagotto E., *Phys. Rev. Lett.*, **87** (2001) 277202.

[19] Ahn K. H., Lookman T. and Bishop A. R., *Nature*, **428** (2004) 401.

[20] Caciuffo R., Rinaldi D., Barucca G., Mira J., Rivas J., Senaris-Rodriguez M. A., Radaelli P. G., Fiorani D. and Goodenough J. B., *Phys. Rev. B*, **59** (1999) 1068.

[21] Kuhns P. L., Hoch M. J. R., Moulton W. G., Reyes A. P., Wu J. and Leighton C., *Phys. Rev. Lett.*, **91** (2003) 127202.

[22] Wu J., Lynn J. W., Glinka C., Burley J., Zheng H., Mitchell J. F. and Leighton C., *Phys. Rev. Lett.*, **94** (2005) 037201.

[23] Phelan D., Louca D., Rosenkranz S., Lee S.-H., Qui Y., Chupas P. J., Osborn R., Zheng H., Mitchell J. F., Copley J. R. D., Sarrao J. L. and Moritomo Y., *Phys. Rev. Lett.*, **96** (2006) 027201.

[24] Phelan D., Louca D., Kamazawa K., Lee S.-H., Ancona S. N., Rosenkranz S., Motome Y., Hundley M. F., Mitchell J. F. and Moritomo Y., *Phys. Rev. Lett.*, **97** (2006) 235501.

[25] Aarbogh H. M., Wu J., Wang L., Zheng H., Mitchell J. F. and Leighton C., *Phys. Rev. B*, **74** (2006) 134408.

[26] Wu J., Zheng H., Mitchell J. F. and Leighton C., *Phys. Rev. B*, **73** (2006) (R)020404.

[27] Woodfield B. F., Wilson M. L. and Byers J. M., *Phys. Rev. Lett.*, **78** (1997) 3201.

[28] Cornelius A. L., Light B. E. and Neumeier J. J., *Phys. Rev. B*, **68** (2003) 014403.

[29] Smith R. X., Hoch M. J. R., Kuhns P. L., Moulton W. G., Reyes A. P., Boebinger G. S., Mitchell J. and Leighton C., *Phys. Rev. B*, **78** (2008) 092201.

[30] Giblin S. R., Terry I., Clarke S. J., Prokscha T., Prabhakaran D., Boothroyd A. T., Wu J. and Leighton C., *Europhys. Lett.*, **70** (2005) 677.

[31] Giblin S. R., Terry I., Prabhakaran D., Boothroyd A. T. and Leighton C., *Phys. Rev. B*, **79** (2009) 174410.

[32] Podlesnyak A., Russina M., Furrer A., Alfonsov A., Vavilova E., Kataev V., Buchner B., Strassle Th., Pomjakushina E., Conder K. and Khomskii D. I., *Phys. Rev. Lett.*, **101** (2008) 247603.

[33] Similar results are obtained in lattice models of microemulsions for example: Andelman D., Cates M. E., Roux D. and Safran S. A., *J. Chem. Phys.*, **87** (1987) 7229.